Correlation of the low and high frequency fatigue responses of pure polycrystalline copper with mechanisms of slip band formation

Nicolas Marti, Véronique Favier, Fabienne Grégori, Nicolas Saintier

Correlation of the low and high frequency fatigue responses of pure polycrystalline copper with mechanisms of slip band formation

Nicolas Marti [a,b,c], Veronique Favier [a,*], Fabienne Gregori [b], Nicolas Saintier [c]

[a] Laboratoire PIMM, Arts et Metiers Institute of Technology, CNRS, CNAM, HESAM Universite, 151 Boulevard de L'Hôpital, 75013, Paris, France
[b] LSPM, Université Paris 13, Sorbonne Paris Cité, CNRS, 99 Avenue Jean-Baptiste Clément, 93430, Villetaneuse, France
[c] I2M, Arts et Metiers Institute of Technology, CNRS, HESAM Universite, Esplanade des Arts et Métiers, 33405, Talence, France

ARTICLE INFO

Keywords:
Fatigue
Ultrasonic frequency testing
Plasticity
Dislocations
Vacancies
Copper

ABSTRACT

Ultrasonic fatigue testing at 20 kHz was developed to accelerate fatigue tests and explore the very high cycle fatigue range. However, the use of ultrasonic fatigue systems raises the open question of the impact of frequency on the material fatigue response. In this paper, the impact of the loading frequency on the fatigue response of face-centered cubic polycrystalline copper is investigated. Firstly, experiments with conventional fatigue devices inducing loading frequencies lower than 100 Hz were carried out and compared with previously published results obtained with an ultrasonic fatigue machine at 20 kHz. At a stress amplitude of 100 MPa, the number of cycles required for failure was found to be more than 200 times greater for tests at 20 kHz than for tests at frequencies below 100 Hz. Secondly, for both types of fatigue tests, the conditions in stress amplitude and number of cycles needed for the emergence of the early slip markings were investigated. The early slip marking S–N curve was found to have the same sensitivity as the failure S–N curve to the frequency effect. Thirdly, the different possible reasons responsible for this frequency effect are discussed. It is concluded that the physical mechanisms of slip marking formation is preserved while their kinetics is sensitive to the loading frequency. Finally, two simplified models were considered and for the first time, the frequency effect on the fatigue response of copper is quantitatively correlated with the occurrence of time-dependent dislocations cross slip and vacancies production/diffusion involved in the persistent slip band formation for face-centered cubic structure. The obtained results could be extended to a full class of materials where slip band formation plays a key role in the crack initiation process while suggesting no frequency effect for materials with a lower degree of plasticity development at crack initiation (High Strength Steels for example).

1. Introduction

Frequency effects on the fatigue response of metals and alloys remain a present and controversy question. The latter became even more relevant by the development of ultrasonic tpefatigue systems allowing fatigue tests at 20 kHz and so strongly reducing the test duration with regard to conventional fatigue machine working at frequencies below 100 Hz. Some alloys are not (or less) sensitive to loading frequency such as face-centered cubic (f.c.c.) nickel-based Udimet 500 [1], f.c.c. AlZnMgCu1.5 aluminium alloy [2] or Ti–6Al–7Nb titanium alloy with hexagonal close-packed (h.c.p) α phase and body-centered cubic (b.c.c.) β phase [3]. Others are sensitive to loading frequency such as b.c.c. tantalum [3], two-phase Ti–6Al–4V titanium alloy [4], b.c.c. low carbon steel [5] or dual-phase steel [6].

Concerning pure polycrystalline copper (f.c.c. structure), the failure S–N curve was determined at frequencies $\leq$100 Hz [7–11], around 1000 Hz [12] and around 15–20 kHz [11,13–16]. Unless otherwise specified, the literature data presented in the following concern annealed copper. The existing literature on the fatigue behavior of annealed copper mostly investigated the effect of heat treatment and mean grain size but very few results allow a direct evaluation of the frequency effect. Thompson and Backofen [7] studied mean grain size effect (ranging from 3 μm to 150 μm) at 30 Hz. Lukáš and Kunz [10] investigated mean grain sizes of 70 μm and 1.2 mm at 100 Hz fatigue frequency. Lukáš et al. [9] worked on 200 μm mean grain size and 80 Hz fatigue loading. The S–N curves are all consistent and show a mean grain

* Corresponding author.
E-mail addresses: nicolas.marti@gadz.org (N. Marti), veronique.favier@ensam.eu (V. Favier), fabienne.gregori@univ-paris13.fr (F. Gregori), nicolas.saintier@ensam.eu (N. Saintier).

size effect for the same loading frequency. Nevertheless, none frequency effect can be deduced from comparisons between these fatigue data as the studied copper polycrystals all have various grain sizes. For 15–20 kHz fatigue loadings, the self-heating of the specimen is generally reduced thanks to a cooling system [15–17] or to the use of a pulse-pause loading [11,13-14].

Phung et al. [15] investigated an annealed copper having a mean grain size of 30 μm cyclically loaded at 20 kHz. They found a S–N curve in very good agreement with the S–N curve obtained by Stanzl-Tschegg et al. [13-14] for an annealed copper with a mean grain size of 60 μm and a similar fatigue frequency. However, stretched copper with a mean grain size of 50 μm showed higher fatigue strength [18]. Awatani et al. [16] demonstrated higher fatigue strength for stretched copper specimens than annealed copper specimens with mean grain size between 100 μm–300 μm and for tests at 17.7 kHz. Moreover, Thompson et al. [12] have shown, in fatigue tests carried out at a frequency of 1000 Hz that the fatigue strength depends on the annealing. All of these literature results demonstrate that the frequency effect must be investigated on the same copper polycrystal since the fatigue response depends on the grain size and thermomechanical history of the material.

Lukáš et al. [17] studied the 100 Hz and 20 kHz fatigue response of copper polycrystals with a mean grain size of 50 μm–70 μm. They found that the fatigue life was longer at 20 kHz than 100 Hz for the same stress amplitude. However, they attributed this result to the fact that the specimens were obtained from different batches rather than a frequency effect. Some remarks on frequency effect on the S–N curve can be found in some papers while this effect was not fully investigated. For instance, Awatani et al. [16] indicated that the fatigue life at 17.7 kHz is six times higher than the fatigue life at 50 Hz. Thompson et al. [12] mentioned that it was not relevant to compare results for different grain sizes obtained in literature when they were not obtained for the same test frequency. Very recently, Stanzl-Tschegg [11] compared the S–N curves obtained at 20 Hz and 19 kHz using similar specimen geometries and pulse-pause loading. They also found that the 19 kHz curve was shifted by about two decades to the largest number of cycles. However, no clear conclusion regarding this frequency effect has been provided.

The fatigue life in high cycle fatigue (HCF) is controlled by the crack initiation stage. In the case of very high cycle fatigue (VHCF), the crack initiation stage is much longer and constitutes more than 90% of the fatigue life [19]. In pure copper, cracks initiate at the surface (type I material, in accordance with the classes defined by Mughrabi) owing to the accumulation of irreversible plastic deformation in slip bands and the formation of extrusions [20-21]. Type I materials are opposed to type II materials where the main crack initiates from an internal defect [20].

In this paper, the authors focus on the frequency effect on the early slip markings in the case of pure copper. A numerical approach to better understand and identify the underlying physical mechanisms is proposed. In this context, further aspects of frequency effects on slip band development, slip localization to micro-crack transition and micro-crack propagation over initial microstructural barriers will not be addressed in this paper. The presented results complements the experimental failure S–N curves obtained at 20 kHz in Ref. [15] with results obtained at 20 Hz in HCF and VHCF for the same polycrystalline copper to study frequency effects on fatigue response. The early slip markings observed at the surface of the specimens were investigated for cyclic loading tests at 100 Hz and compared to those obtained at 20 kHz, to correlate fatigue frequency effects to the mechanisms of slip bands formation. The different possible origins of the frequency effect are discussed. For the first time, two models based on cross slip of screw dislocations and production/diffusion of vacancies were developed to successfully quantify the experimentally observed frequency effect.

2. Experimental procedure

2.1. Material

The material of the study is an Oxygen-Free High Conductivity (OFHC) polycrystalline copper (more than 99.95% purity) supplied by Griset company in France. This material was chosen for its simple microstructure compared to industrial materials and is one of the reference materials in literature. The material was received in the form of hot rolled plates and is composed of equiaxed grains (Fig. 1). The mean grain size is 30 μm and the crystallographic textures induced by manufacturing are moderately marked (the maximum texture index level on pole figures is about 3). About 35% of the grain boundaries are coherent Σ3 twin boundaries, the twin plane is {1 1 1}.

Concerning its mechanical features, the static yield strength defined for a plastic strain of 0.2% is about 75 MPa. However, due to cyclic hardening, the strength of the material reaches about 120 MPa for 0.2% strain amplitude [22-23]. The Young's modulus was determined through a vibration test performed with an ultrasonic fatigue machine. The experimental procedure consists in identifying the length L of a cylindrical copper specimen that allows its lowest resonant frequency associated with the longitudinal vibration mode to be equal to ~20 kHz corresponding to the working frequency of the ultrasonic fatigue machine. The Young's modulus E can be analytically computed with the relation $E = 4f^2L^2\rho$ where ρ is the measured density. The resulting Young's modulus is about 130 GPa. This value is in good agreement with literature [14] and was considered for all calculations (in particular for the design of the specimens) and fatigue tests whatever the loading frequency.

Uniaxial compression tests at various strain rates were carried out on 6 mm diameter – 6 mm height cylindrical copper specimens to investigate the strain rate sensitivity of the studied material. A servo-hydraulic MTS machine was used to investigate strain rates ranging from 10^{-4} to 10^{-1} s^{-1}. Hopkinson bars were used to reach strain rates ranging from 500 s^{-1} to 3000 s^{-1}. The true stress σ as a function of the strain rate $\dot{\varepsilon}$ for three strain values ($\varepsilon = 0.05, 0.1, 0.2$) is plotted in Fig. 2. The obtained linear relationship is characterized by its slope, namely the strain rate sensitivity index defined as $m = \partial log(\sigma)/\partial log(\dot{\varepsilon})$. The value of m is about 0.01. This value is low as expected for face-centered cubic structure and in good agreement with literature for similar grain size copper loaded at room temperature [24-25].

2.2. Fatigue tests, facilities and specimens

Tests at "low" frequencies (20 Hz and 100 Hz) were carried out in

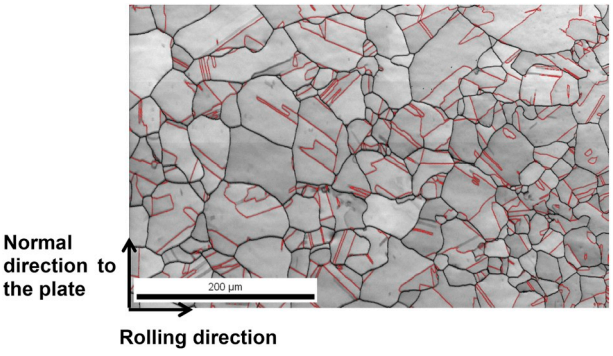

Fig. 1. Grain map of the studied polycrystalline pure copper obtained by quality index analyses in the normal direction – rolling direction plane determined by EBSD. Dark lines correspond to the grain boundaries and superimposed lighter grey lines (or red in online version) correspond to the computed twin boundaries. (For interpretation of the references to colour in this figure legend, the reader is referred to the Web version of this article.)

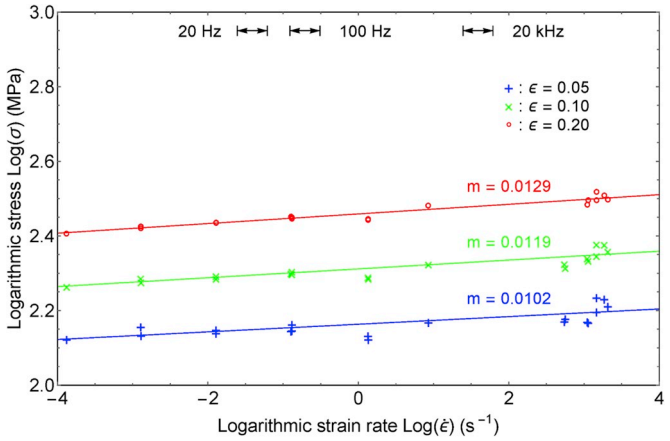

Fig. 2. Stress-strain rate curves for three strain values ($\varepsilon = 0.05$, 0.1, 0.2) in a logarithmic scale and the associated strain rate sensitivity index $m = \partial log(\sigma)/\partial log(\dot{\varepsilon})$. The mean strain rate $\widetilde{\dot{\varepsilon}}$ ranges occurring for 20 Hz, 100 Hz and 20 kHz fatigue loadings are indicated at the top of the figure (these strain rates $\widetilde{\dot{\varepsilon}}$ were computed on the basis of stress amplitudes σ_a applied in our fatigue tests and assuming an elastic behavior, as given by Eq. (1), section 4.3).

fully reversed sinusoidal tension-compression loadings (the load ratio $R = -1$) with constant amplitude with different facilities: a servo-hydraulic machine for the 20 Hz test set up in the Technical Centre for Mechanical Industry in France (CETIM) and an electromagnetic machine for the 100 Hz tests. Tests at "high" frequencies and more specifically at ~20 kHz were performed with an ultrasonic machine. These tests at 20 kHz were done in a previous study on the same material [15]. Experimental techniques for tests at "low" frequencies are well known and are not detailed here. They are referred to as "conventional" machines in the subsequent text. For "high" frequency tests which use the less common ultrasonic machine, details are given hereafter and the characteristics of the tests carried out by "conventional" and "ultrasonic" machines are indicated.

The ultrasonic machine is composed of a piezoelectric transducer which converts an electrical signal into a mechanical longitudinal sinusoidal displacement with a frequency of about 20 kHz. This displacement is amplified via a horn and transmitted to the specimen. The latter is designed to have its lowest resonant frequency associated with the longitudinal vibration mode at the excitation frequency of the piezoelectric transducer (free vibration at 20 kHz in our case). Thus, one of the differences between tests at "low" and "high" frequencies is that the force is imposed for tests at "low" frequencies while an electrical signal is given for tests at "high" frequencies. However, as the piezoelectric transducer response is linear, the displacement can be considered as the input of the fatigue test. In addition, given the fatigue life span involved in this work, it is reasonable to consider that the material behavior is linear elastic at the macro scale, at least during the crack initiation stage. Consequently, the two loading conditions (force and displacement) of the two fatigue devices are equivalent and do not induce bias in the result analyses.

In the case of "high" frequency tests, specimens were designed using a one-dimensional dynamic beam model assuming a pure linear elastic behavior. This model allows to estimate the stress amplitudes along the specimen for a given displacement. To impose accurately the level of loading in the high frequency specimens, a calibration procedure was performed at the beginning of each test series with strain gages at the center of the specimen gage length. Thereafter, stress amplitudes were computed from measured strains (assuming an elastic behavior) and correlation was made between the imposed displacement (or electrical tension) and the corresponding local stress along the specimen. The determination of the local stress for the low frequency tests does not represent any difficulty in itself. However, since high frequency specimen geometries induce specific stress gradients along the specimen axis, a particular attention was given to their design in order to obtain similar stress distribution in the specimen gage length independently of the test frequency (Fig. 3 and Fig. 4).

S–N curves were obtained from cylindrical hourglass shaped specimens while flat hourglass shaped specimen were preferred to carry out surface observations after interrupted fatigue tests. Fig. 3c) and Fig. 4c) show the stress amplitude profile along the specimen axis for cylindrical specimens (used for tests at 20 Hz and 20 kHz) and flat specimens (used for tests at 100 Hz and 20 kHz). Specimen geometries for each frequency are given in Fig. 3ab) and Fig. 4ab). All specimens were polished mechanically and electrochemically before tests. The transient regime represents about 10^3 cycles for all the tests (checked with a laser interferometer for tests). Besides, at "low" frequencies the self-heating of the specimen is negligible (less than 1 °C) To prevent from any temperature impact on mechanical properties, specimens were cooled by pulsed air during tests at 20 kHz [15]. In all cases, the temperature of the specimens during the fatigue tests remained close to room temperature. A comparison of the loading conditions for "low" and "high" frequency tests is given in Table 1.

2.3. Investigation of early slip markings

The numbers of cycles needed to form the early slip markings as a function of the stress amplitude were determined for 100 Hz fatigue tests and compared with literature data. These literature data were obtained on the same material but with 20 kHz fatigue tests by a previous study in

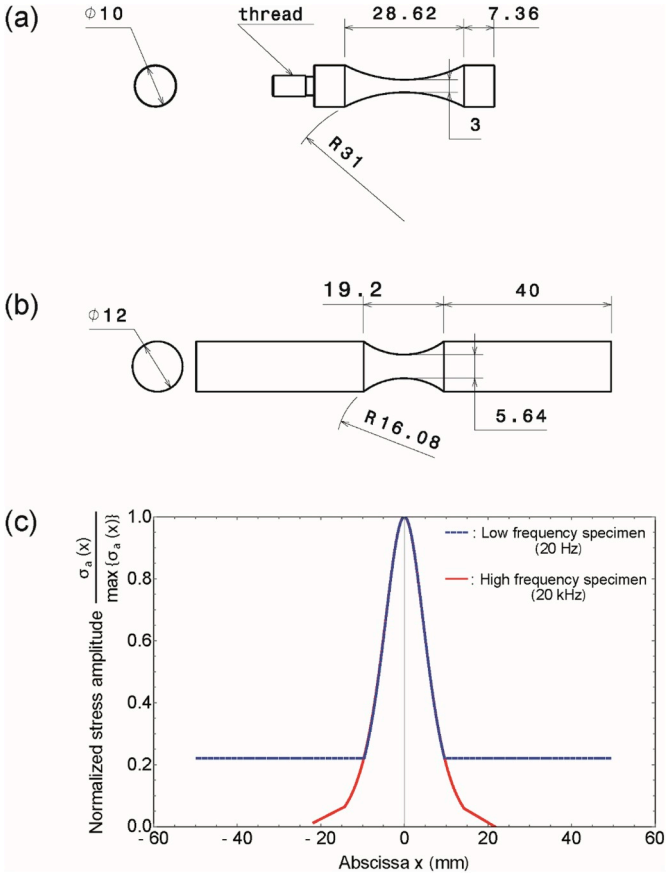

Fig. 3. Geometry and stress amplitude profile for cylindrical specimens (dimensions in mm) (a) hourglass specimen geometry for the 20 kHz ultrasonic machine – (b) hourglass specimen geometry for the 20 Hz servo-hydraulic fatigue machine – (c) normalized stress amplitude profile along the specimen axis for cylindrical specimens designed for the 20 kHz ultrasonic fatigue machine (line) and 20 Hz servo-hydraulic fatigue machine (dashed line).

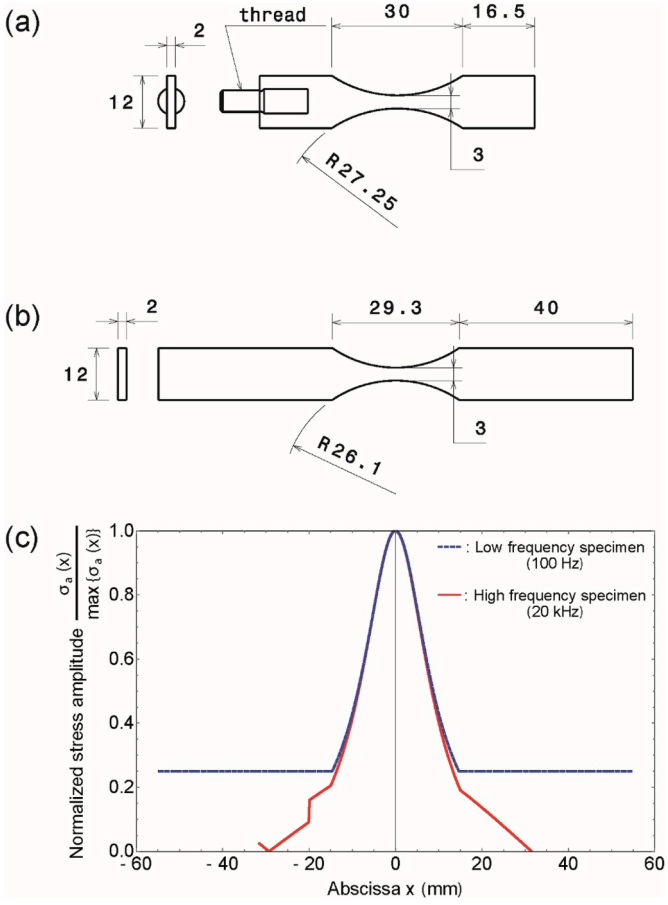

Fig. 4. Geometry and stress amplitude profile for flat specimens (dimensions in mm) (a) hourglass specimen geometry for the 20 kHz ultrasonic machine – (b) hourglass specimen geometry for the 100 Hz electromagnetic fatigue machine – (c) normalized stress amplitude profile along the specimen axis for flat specimens designed for the 20 kHz ultrasonic fatigue machine (line) and 100 Hz electromagnetic fatigue machine (dashed line).

Table 1
Comparison of the loading conditions for "low" and "high" frequency tests.

	"Low" frequency tests	"High" frequency tests
Vibration	Forced	Free
Use of cooling system	No	Yes
Control	Force-controlled and considered stress-controlled	Electrical signal-controlled and considered displacement-controlled and stress-controlled
Duration of transient state	About 10^3 cycles	About 10^3 cycles
Calibration	With strain gages	With strain gages
Parasitic loads	Estimated with strain gages and with the sensors of the machine (see paragraph 4.2)	Estimated with strain gages, with laser interferometer and with finite element computations (see 4.2)

the laboratory [15]. For each stress amplitude, the test was regularly interrupted to observe the slip markings on the specimen surface. The observations were performed in the center of the specimens and more precisely in a 3 mm long region, where the stress amplitude is maximum and can be considered uniform (see Fig. 4). As soon as an early slip marking was observed by optical microscope, the number of cycles at which the test was stopped was registered. The previous number of cycles at which no slip marking was observed was also registered. The two numbers of cycles provide the range of number of cycles in which an early slip marking appeared. It is called Slip Marking Cycle Range (SMCR) in the following. The stress amplitude range [45 MPa–85 MPa] was chosen to match the stress amplitude-number of cycles domains investigated in both conventional and ultrasonic fatigue tests.

3. Results

3.1. Failure: S–N curves

Fig. 5 illustrates fatigue test results at 20 Hz and 20 kHz [15] together with fatigue test results at 100 Hz obtained with flat specimens in this work. Considering the natural dispersion of fatigue processes, it can be considered that the results obtained at 20 and 100 Hz are very similar whatever the shape (flat or cylindrical) of the specimen. These results can be unified using a single master S–N curve. To simplify, 20 and 100 Hz are called "low" frequencies and 20 kHz is called "high" frequency in the following. The "low" frequency failure S–N curve exhibits two regimes. The S–N curve slope is - 25 MPa per decade of number of cycles for [8×10^4 - 3.7×10^6] cycles and [75–120] MPa stress amplitudes. For stress amplitudes below 75 MPa and number of cycles above 3.7×10^6, the slope becomes very slight and tends to a plateau at about 75 MPa. The "high" frequency failure S–N curve also displays two regimes for which the stress amplitude linearly decreases with number of cycles. The slope is about -5.3 MPa per decade of number of cycles for [3.6×10^6–5×10^7] cycles and [97–115] MPa stress amplitudes. For stress amplitudes below 97 MPa and number of cycles above 1×10^8, the slope becomes very low about -0.4 MPa per decade of number of cycles. At amplitude of 91 MPa, failure did not occur up to 5.4×10^9 cycles at which tests were stopped [15]. These results are in very good agreement with previously obtained experimental results on similar pure polycrystalline copper for "high" [13-14] and "low" frequencies [11].

The failure S–N curves reveal a significant frequency impact on the behavior of polycrystalline copper under fatigue loading: for a given number of cycles, the fatigue strength is higher at "high" than "low" frequencies, and for a given stress amplitude, the fatigue life is higher at "high" than "low" frequencies. Table 2 shows the ratio of "high" frequency fatigue life to "low" frequency fatigue life at four various stress amplitudes. The ratio clearly increases with decreasing stress amplitudes revealing that the frequency effect is more pronounced when the stress amplitude is low.

The crack leading to the final failure was found to systematically initiate from the surface of the specimens. Similar results were found for fatigue tests at 20 kHz [15].

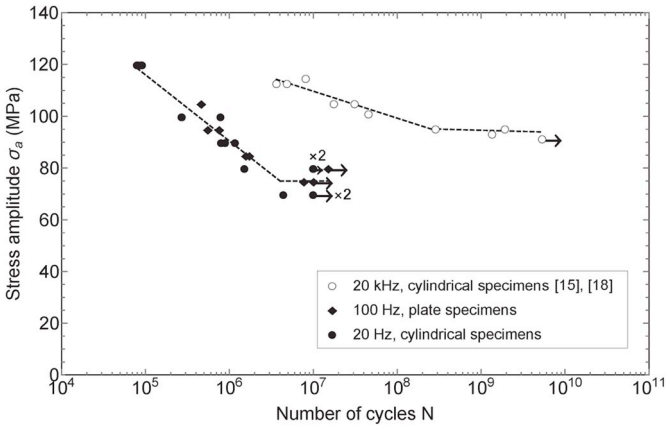

Fig. 5. Stress-Number of cycles to failure curve for pure polycrystalline copper obtained after "high" frequency fatigue tests (open dots) and "low" frequency fatigue tests (black dots).

Table 2
Ratio of "high" frequency fatigue life to "low" frequency fatigue life at four various stress amplitudes.

Stress amplitudes σ_a(MPa)	Ratio of the fatigue life at "high" frequency to the fatigue life at "low" frequency (decades)
115	1.5
105	2.1
95	2.7
94	3.9

3.2. Early slip markings: S–N curve and morphology

As mentioned in Section 2.3, the numbers of cycles needed to form the early slip markings as a function of the stress amplitude were determined for 100 Hz fatigue tests to be compared with literature data obtained at 20 kHz fatigue tests from Ref. [15]. The results leading to the so-called early slip marking S–N curves are presented in Fig. 6. The horizontal bars represent the SMCR at each investigated stress amplitude levels. The number of cycles needed to initiate slip markings increases with decreasing stress amplitude for both frequencies. However, as for the failure S–N curves, the number of cycles is higher at high than low frequency for a given stress amplitude.

In the [45 MPa–85 MPa] range studied here, the early slip markings observed at 100 Hz cyclic loading are straight. They are isolated as illustrated in Fig. 7a). They are inclined ~45° (±15°) from the loading axis. The morphology and location of the early slip markings observed after 20 kHz cyclic loading were reported in Ref. [15]. In the [45 MPa–65 MPa] range, the early slip markings are very similar to the early slip markings observed in the present study, as illustrated in Fig. 7b). These slip markings were labelled as slip markings of type II and are considered as persistent slip bands (PSB) since they re-appear after new polishing and cycling [15]. Optical micrograph in Fig. 8a) shows early slip markings observed after 5000 cycles for 85 MPa stress amplitude and 100 Hz frequency. Here again, isolated and straight slip markings oriented at about 45° from the loading direction were observed. Fig. 8bcd) present the same zone but after 10^6 cycles. More slip markings were observed. Most of them are slip markings of type II. EBSD images demonstrate that they are located very near and along twin boundaries (Fig. 8d). However, slip markings crossing grains were also observed (Fig. 8c). This other type of slip markings was also observed at 20 kHz [15] at stress amplitude close to 85 MPa and was labelled as slip markings of type I.

Most of slip markings of type I and II observed after "low" frequency tests exhibit clear extrusions in their center as illustrated in Fig. 8e). Some intrusions were also observed but much more rarely (Fig. 8f). For "high" frequency tests, central extrusions were also clearly observed by scanning electron and atomic force microscopies for the types I and II of slip markings [15].

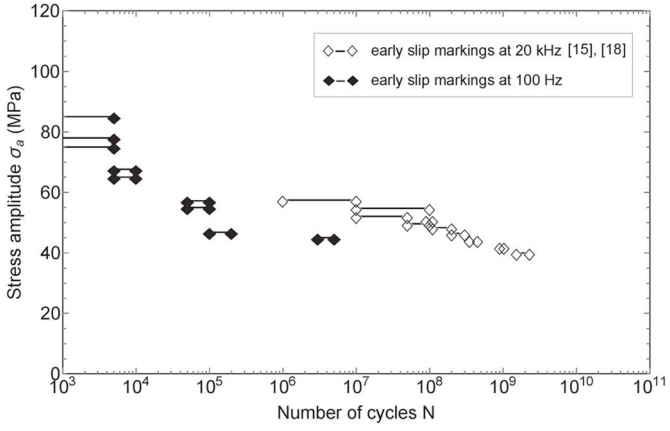

Fig. 6. Stress amplitude needed to form the early slip markings as a function of the number of cycles (S–N early slip marking curves).

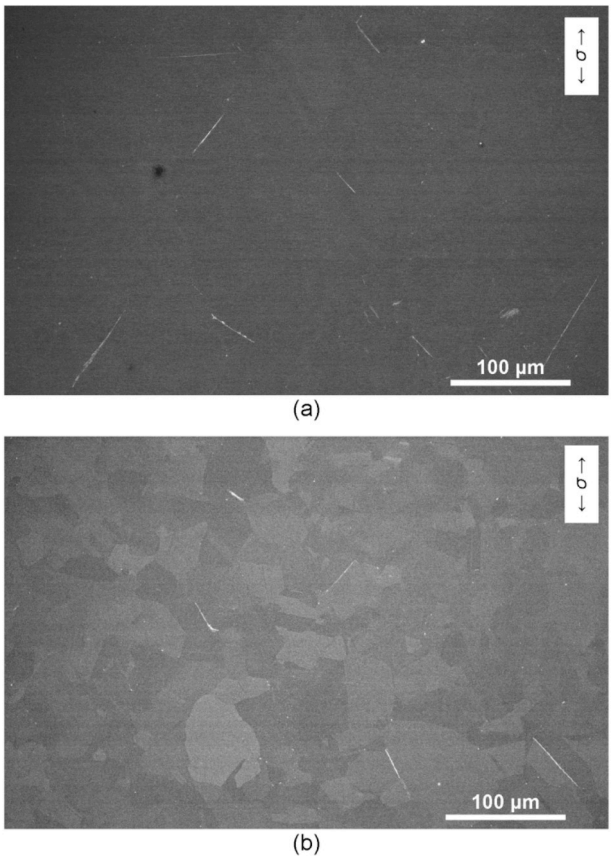

Fig. 7. Scanning electron micrograph of typical early slip markings (white straight lines) observed after 10^6 cycles at 65 MPa stress amplitude – a) 100 Hz loading - b) 20 kHz loading.

4. Discussion

4.1. Summary of the results

The failure and early slip marking S–N curves are clearly different when determined at "low" and "high" frequencies. For failure S–N curves, the fatigue strength and life were found higher at "high" than "low" frequencies. The early slip markings were also found to emerge at a higher number of cycles (resp. stress amplitude) for a given stress amplitude (resp. number of cycles) when the frequency increases from 100 Hz to 20 kHz. These similar tendencies suggest a correlation between both failure and early slip marking S–N curves. The existence of such correlation is a reasonable hypothesis as it is well-known that formation and emergence of slip bands play a key role in crack initiation and fatigue failure in ductile single-phase metals [26]. Further aspects of frequency effects on slip band development, slip localization to micro-crack transition and micro-crack propagation over initial microstructural barriers could also be frequency sensitive but are not be addressed in this paper. The discussion focusses on the early slip band emergence.

The observations of the surface of the fatigued specimens revealed that the morphology and location of the early slip markings were the same for "low" and "high" frequencies. The early slip markings were mainly located close to ~45° inclined twin boundaries. This type of slip markings was already observed in literature after fatigue loading at frequency lower than 100 Hz and low stress amplitudes with regard to the "conventional fatigue limit" determined at 10^7 cycles [27–30].

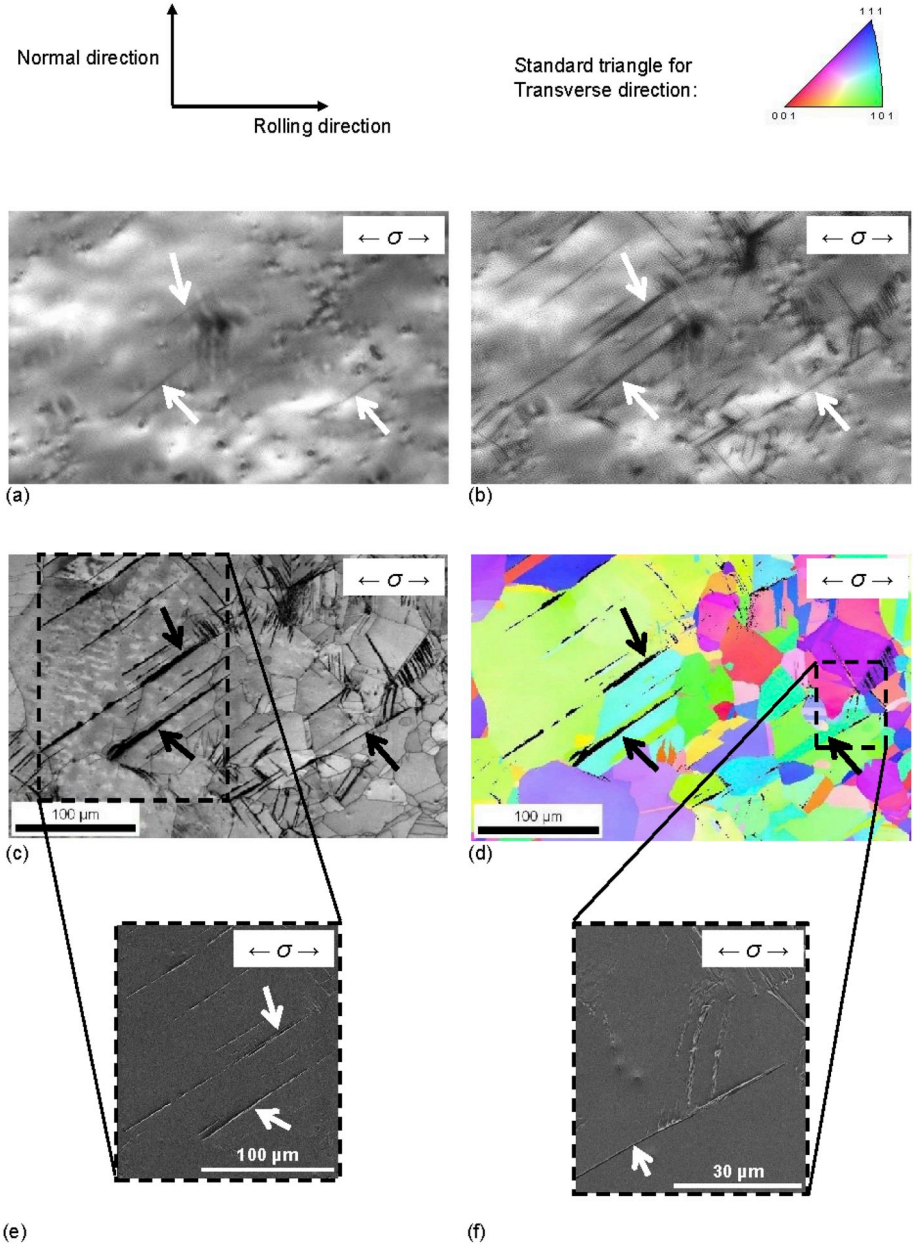

Fig. 8. (a) Optical micrograph of typical early slip markings observed after 5000 cycles for 85 MPa stress amplitude and 100 Hz cyclic loading – (b) Same specimen zone observed after 10^6 cycles – (c) same as (b) with the same scale but observed using EBSD index of quality – (d) same as (b) and (c) with the same scale but grain map from EBSD analyze – (e) higher magnification of (c) showing slip markings observed with scanning electronic microscope – (f) higher magnification of (d) showing slip markings observed with scanning electronic microscope. The arrows indicate some specific slip markings.

Well-oriented twin boundaries are indeed preferential sites for appearance of early slip markings at very low stress amplitudes because of strong stress concentrations induced by elastic anisotropy at the grain scale (cubic elasticity) and the existence of well-oriented slip planes parallel to the twin boundary plane [31]. Besides, for "low" and "high" frequencies, similar changes of the specimen surface relief during cycling were observed: growth of extrusions and increase in number of slip bands.

From the above mentioned observations, it can be concluded that the frequency does not affect significantly the morphology and location of slip markings. The physical mechanisms of slip marking formation seem preserved while their kinetics is modified. Several reasons may explain the frequency sensitivity of the kinetics of slip band formation. Firstly, the fatigue system is different for "low" and "high" frequencies which may slightly change the loading conditions. Secondly, the strain rate sensitivity of material behavior leads to increase the yield stress at high frequency. Thirdly, the testing time is higher at "low" than "high" frequency. Consequently, time-dependent mechanisms involved in fatigue may be sensitive to the duration of the test. Fourthly, when no cooling system is used, the self-heating of the specimen due to intrinsic dissipation can be much higher at "high" than "low" frequencies [32]. Roth et al. [33] indicated that the self-heating of copper specimen affected the fatigue lifetime of copper. As mentioned in Section 2.2, a cooling system was used for the 20 kHz test so that the temperature of the specimens during all the fatigue tests remained close to room temperature. Consequently, the impact of temperature was considered as negligible in this study. The other three first origins are discussed in the following.

4.2. *Fatigue machines at 100 Hz and 20 kHz cyclic loadings*

In both cyclic tests at 100 Hz and 20 kHz, the specimen oscillate and the overall system composed of the machine and specimen can be represented by a spring to model the elastic stiffness coupled with a dashpot to mimic the damping phenomena related to the machine and/or to the specimen such as internal friction and micro-plasticity. When the early slip markings emerge to the surface, the micro-plasticity remains very low so that a pure linear elastic behavior and so a linear relationship between stress and strain can be considered at the scale of the specimen.

Consequently, although the 100 Hz tests were load-controlled while the 20 kHz tests can be considered as displacement-controlled (see Section 2.2), this effect on the stress amplitude estimation was neglected. Besides, because of the specific design of the specimens, the same stress amplitude gradient along the specimen axis takes place for a given stress or displacement amplitudes. In addition, size effect is negligible because the volumes tested are similar.

For both types of fatigue tests, torsion and bending parasitic loads could occur. In the case of electromagnetic and servo-hydraulic machines, they can be due to a slight misalignment between the two jaws. In the case of ultrasonic machine, bending parasitic vibrations could take place when the natural frequency of the bending vibrations is close to 20 kHz. For flat specimens, the bending strains were measured by means of strain gages stuck on each side of a specimen. In the case of "low" frequency tests, the corresponding static bending stresses were estimated to ±15 MPa. The dynamic bending stresses were estimated lower than 2 MPa. In the case of 20 kHz tests, no significant bending strain was measured. For cylindrical specimens and "high" frequency tests, the bending was quantified by measuring the displacements in the bending antinodes with a laser interferometer. They were found negligible. For "low" frequency tests, an alignment of the two jaws was performed to reduce bending effects. For the torsion stresses, as far as ultrasonic machine tests are concerned, torsion vibrations measured by the laser were undetectable showing that their magnitude was very slight. For "low" frequency tests, they were calculated from the measurement of the torsion moment. The static ones were found lower than 9 MPa and the dynamic ones ~6 times lower than the axial stresses. These results show that these irregular stresses are lower but not negligible than the axial stresses ranging from 45 MPa to 120 MPa. Thus, the torsion and bending irregular stresses could increase the true stress amplitude applied to the specimen and so reduce the discrepancy in stress between the two early slip bands curves. However, the number of cycles needed to get the early slip bands remains much lower at 100 Hz than 20 kHz.

4.3. Strain rate sensitivity

The strain rate sensitivity of copper is low in the [10^{-4} s^{-1} - 10^{3} s^{-1}] strain rate range (see Section 2.1) as expected for f.c.c. ductile materials. As the strain rate value varies sinusoidally with time from 0 to a maximum value during one cycle, the absolute mean value of the strain rate during one cycle of period τ was considered to estimate the impact of the strain rate on the flow stress. It is given by:

$$\tilde{\dot{\varepsilon}}(f) = \frac{1}{\tau}\int_0^{\tau} |\dot{\varepsilon}(t)| dt = 4f\frac{\sigma_a}{E} \qquad \text{Eq. 1}$$

For the same stress amplitude σ_a, changing the frequency f from 100 Hz to 20 kHz results in increasing 200 times the strain rate. In order to assess the impact of the strain rate sensitivity on the failure and early slip marking S–N curves, the stress amplitude was normalized by the flow stress at arbitrary 5% plastic strain associated with the strain rate calculated using Eq. (1). Fig. 9 shows the evolution of the normalized stress amplitude as a function of the number of cycles. The data obtained at both frequencies are closer than in Fig. 6 but the remaining discrepancy suggests that the impact of strain rate cannot explain alone the higher stress amplitude or number of cycles found at 20 kHz with regard to those obtained at100 Hz. This conclusion was also suggested by Roth et al. [33].

4.4. Time-dependent mechanisms

To investigate possible time effect, Fig. 6 was replotted by considering time rather than number of cycles for the *x*-axis (Fig. 10). The data obtained at 100 Hz overlap very well with those obtained at 20 kHz. This result reveals that the differences in the early slip band curves found in Fig. 6 are related to an effect of time. Specifically, the loading time to reach 10^6 cycles at 20 kHz is 200 times shorter than at 100 Hz.

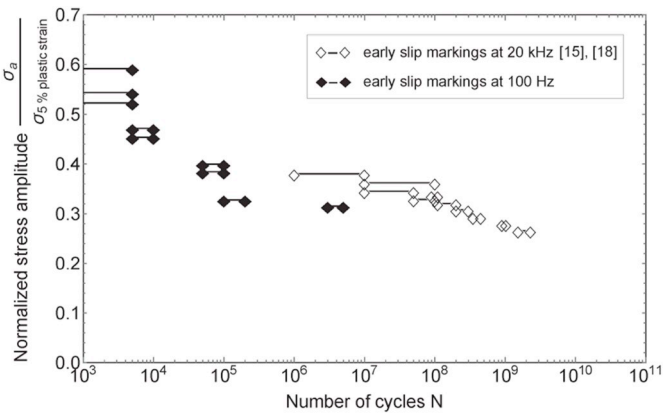

Fig. 9. Early slip marking S–N curves: normalized stress amplitude by the flow stress at 5% plastic strain as a function of number of cycles.

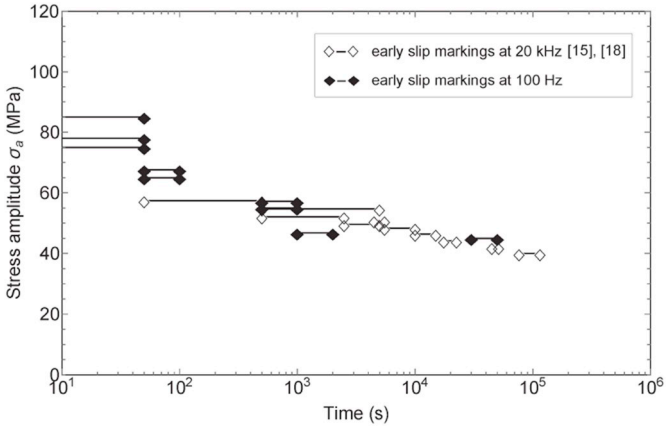

Fig. 10. Early slip marking S–N curves as a function of the duration of test rather than as a function of number of cycles.

From a physical point of view, the initiation of persistent slip bands at the surface of fatigued specimens requires cross slip of screw dislocations to promote slip localization and irreversibility [30,34–36]. In addition, production of vacancies in PSB and their diffusion towards the matrix favor their emergence [37–39]. In this section, firstly a model based on cross slip events for explaining the frequency effect in the early slip marking emergency is presented. Secondly, a model based on production and diffusion of vacancies is proposed.

4.4.1. Model based on cross slip

Cross slip is a thermally-activated mechanism. Its occurrence increases with temperature or when the time let for its occurrence increases. In order to carry out dynamics dislocations (DD) simulations, Déprès et al. [36] represented cross slip events using a stochastic procedure coming from Verdier et al. [40]. The cross-slip probability P is computed as follows:

$$P = \beta\frac{l}{l_0}\frac{\delta t}{t_0}exp\left(\frac{\tau_{css}-\tau_{csR}}{kT}V\right) \qquad \text{Eq. 2}$$

where β is a normalization coefficient ensuring that $0 < P < 1$, $\frac{l}{l_0}$ is the ratio of the length of a screw segment to a reference length l_0=1 mm, $\frac{\delta t}{t_0}$ is the ratio of the considered time to a reference time, V is the activation volume associated to cross slip, $\tau_{css} - \tau_{csR}$ compares the resolved shear stress τ_{css} on the cross slip system to a threshold stress τ_{csR} required to activate cross slip, k is the Boltzmann constant and T the absolute

temperature. It should be noticed that for a given $(\tau_{css} - \tau_{csR})$ the cross slip probability is proportional to δt.

Considering sinusoidal loading stress, it can be easily shown that, during one loading cycle, the duration during which τ_{css} is greater than τ_{csR} is:

$$\Delta t_{1cycle} = \left(1 - \frac{2arcsin\left(\frac{\tau_{csR}}{\tau_{css}}\right)}{\pi}\right)\frac{1}{f} \quad \text{Eq. 3}$$

Assuming that all the parameters of Eq. (2) are frequency insensitive, Eq. (3) shows that the duration Δt_{1cycle} during which τ_{css} is greater than τ_{csR} is 200 hundred times longer at 100 Hz than 20 kHz for a given stress amplitude (same τ_{css}). In other words, during one cycle, the probability to activate cross slip per cycle is 200 hundred times shorter at 20 kHz than 100 Hz. As a result, to obtain the same cumulated probability of cross slip activation during fatigue loading, namely the same duration T_A during which τ_{css} is greater than τ_{csR}, the number of cycles has to be 200 hundred times higher at 20 kHz than 100 Hz as shown by Eq. (4):

$$T_A = \Delta t_{1cycleat100Hz} \times N_{100Hz} = \Delta t_{1cycleat20000Hz} \times N_{20000Hz} \quad \text{Eq. 4}$$

The ratio of the number of cycles to obtain the same cumulated probability of cross slip events is given by:

$$\frac{N_{20000Hz}}{N_{100Hz}} = \frac{\Delta t_{1cycleat100Hz}}{\Delta t_{1cycleat20000Hz}} = 200 \quad \text{Eq. 5}$$

According to this model and considering that the same quantity of cross slip events are required to observe the early slip markings for both frequencies, a discrepancy of $log(200)$=2.3 decades between the number of cycles required for the appearance of the early slip bands exists. Shifting results obtained at 100 Hz to 2.3 decades provides a very good overlap of the results obtained at both frequencies as illustrated in Fig. 11.

4.4.2. Model based on production and diffusion of vacancies

The earliest model based on vacancies to explain the formation of extrusions was proposed by Essman et al. [37]. Only the production of vacancies due to the edge dislocation glide inside persistent slip bands was considered. The extrusion is considered to be due to the additional volume of the produced vacancies. More recently, Polák and Sauzay [39] suggested an analytical model based on the production and migration of point defects (interstitials and vacancies) in PSB. In the present study, as aforementioned observations evidenced for both frequencies (see Section 3.2), the PSB are formed mostly by extrusions in the central part of PSB. This morphology confirms the predominant role of vacancies in transfer of matter within PSB [41]. At temperatures ranging from 80 K to 300 K, the contribution of interstitials to the extrusion growth can be neglected with regard to the role of vacancies [41]. Polák and Sauzay's model [39] assumes that the extrusion growth is due to the production of vacancies in PSB but also their diffusion to the surrounding matrix. This diffusion is indeed balanced by the reversed migration of atoms from the surrounding matrix to the PSB leading to additional matter in the PSB and extrusion growth. Annihilation process of vacancies in PSB is also taken into account. The growth rate of the extrusion per cycle is given as follows:

$$\frac{dh}{dN} = \frac{2pL}{w}\sqrt{\frac{D\tau}{A}}th\left(\frac{w}{2}\sqrt{\frac{A}{D\tau}}\right) \quad \text{Eq. 6}$$

where p is the production rate of vacancies within PSB which strongly depends on the local plastic shear amplitude in the band [38]. L is the depth of PSB below the surface, w is the width of PSB, A is the vacancy annihilation coefficient, and $\tau = 1/f$ is the period of a fatigue cycle. D is the vacancy diffusivity coefficient and is given by:

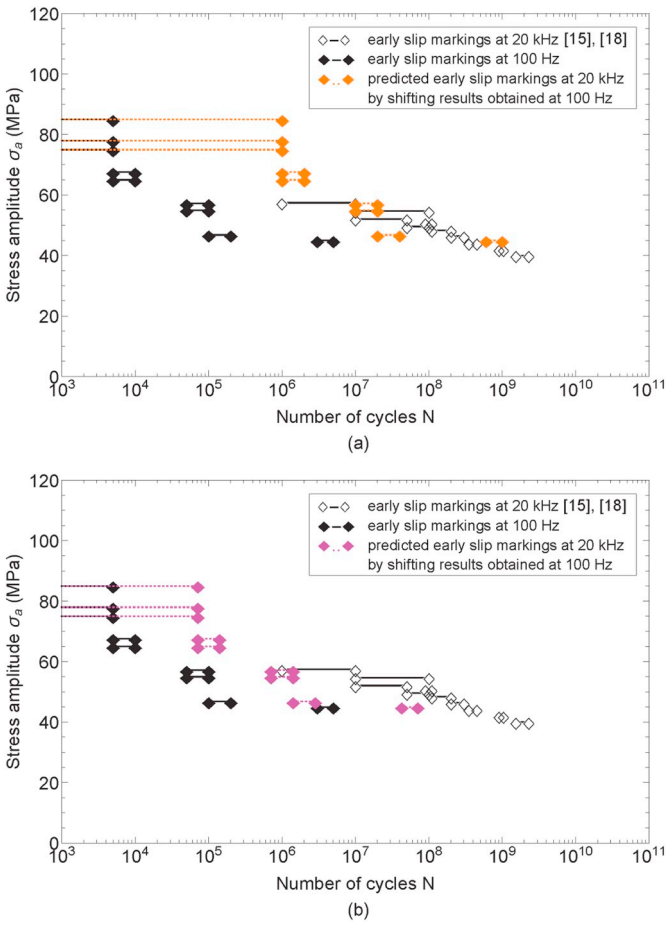

Fig. 11. Early slip marking S–N curves obtained at 100 Hz and 20 kHz for pure polycrystalline copper with black dots for experimental data at 100 Hz, open dots for experimental data at 20 kHz, and (a) predicted data at 20 kHz in dashed orange considering the same cumulated probability for cross slip events to obtain the early slip bands or (b) predicted data at 20 kHz in dashed purple considering the same height of the early slip bands. (For interpretation of the references to colour in this figure legend, the reader is referred to the Web version of this article.)

$$D = \sqrt{6}b^2\nu \times exp\left(\frac{-E_M}{kT}\right) \quad \text{Eq. 7}$$

where b is the distance between neighbor atoms, ν the Debye frequency, E_M the diffusion (migration) energy of vacancies, k the Boltzmann constant and T the absolute temperature. Two extreme cases can be distinguished. For high temperatures where the vacancy mobility is very high, Eq. (6) becomes:

$$\frac{dh}{dN} = pL \quad \text{Eq. 8}$$

It results that the growth rate of an extrusion is insensitive to the frequency. In case of low temperatures corresponding to low vacancy mobility, Eq. (6) is simplified to:

$$\frac{dh}{dN} = \frac{2pL}{w}\sqrt{\frac{D\tau}{A}} \quad \text{Eq. 9}$$

In that case, the growth rate of an extrusion is frequency sensitive. Considering that the plastic shear in the early PSB and their morphology (characterized by w and L) obtained for "low" and "high" frequencies are similar, the three parameters (p, A, E_M) of Eq. (6) to Eq. (9) were assumed to keep the same. Their values were taken from Ref. [39] and are given in Table 3. They are associated to copper polycrystal cyclically loaded in

Table 3
Values of (p, A, E_M) of Eq. (6) and Eq. (7) taken from Ref. [39].

p (/cycle)	A	E_M (eV)
8.9×10^{-7}	2.5×10^{-3}	0.74

low temperature and frequency (0.2 Hz) conditions.

The transition temperature between the two extreme cases was estimated by equating Eq. (8) and Eq. (9) and considering the temperature dependence of the diffusion coefficient (Eq. (7)). In case of copper, the self-diffusion constant $D_0 = \sqrt{6}b^2\nu$ for vacancies and copper atoms is $0.25 \times 10^{-4}\frac{m^2}{s}$ [42]. The width w of PSB was taken equal to 1 μm [15, 39]. The transition temperature was found equal to 433 K at 100 Hz and 591 K at 20 kHz. Consequently, as the temperature of the present fatigue tests was close to room temperature, low temperature conditions are involved and the growth rate of an extrusion is frequency sensitive. All the parameters in Eq. (9) being considered as constant, the growth rate of an extrusion is found to decrease with increasing frequency. The height h of an extrusion as a function of the number of cycles N test can be calculated as

$$h(N) = \alpha \frac{N}{\sqrt{f}} \qquad \text{Eq. 10}$$

where α is constant. Assuming that the early slip bands detected at 100 Hz and 20 kHz have the same critical height h_c, the number of cycles required to reach h_c can be calculated for both frequencies

$$h_c = \alpha \frac{N_{100Hz}}{\sqrt{100}} = \alpha \frac{N_{20000Hz}}{\sqrt{200000}} \qquad \text{Eq. 11}$$

Thus, the ratio of the number of cycles to obtain the same height of an early slip band is given by.

$$\frac{N_{20000Hz}}{N_{100Hz}} = \sqrt{200} \cong 14 \qquad \text{Eq. 12}$$

According to this model and considering that the observed early slip bands have the same height for both frequencies, a discrepancy of $log(\sqrt{200}) = 1.15$ decades between the number of cycles required for the appearance of the early slip bands exists. Shifting results obtained at 100 Hz to 1.15 decades provides a slight overlap of the results obtained at both frequencies as illustrated in Fig. 11.

4.4.3. Synthesis

The strain rate sensitivity of copper is very low and cannot explain alone the reason why the stress amplitude with regard to the flow stress required to get the early slip bands between $10^6 - 10^7$ cycles was found lower at 100 Hz than 20 kHz. In addition, it cannot explain why, for normalized stress amplitude of about 0.3, it takes about a hundred times less cycles to observe the early slip bands at 100 Hz (Fig. 9). On the contrary, Fig. 10 clearly shows a very good agreement between the early slip bands obtained at 100 Hz and 20 kHz when the duration of the tests instead of the number of cycles is taken into account. In other words, the same cycling time is required to get the early slip bands. Two time-dependent mechanisms responsible for strain localization in slip bands and extrusion growth were investigated by means of simplified literature model: cross slip events which promote slip irreversibility and production/diffusion of vacancies in slip bands which promote extrusion growth. The models predict quantitative delay in number of cycles for 20 kHz with regard to 100 Hz fatigue tests. A very good consistency between the data obtained at 100 Hz and 20 kHz has been found when the cumulated probability for cross slip was accounted for. When the production/diffusion was considered, the predicted data at 20 kHz from the experimental ones at 100 Hz were found close to the experimental data at 20 kHz but a slight discrepancy remains.

These results suggest that both mechanisms can explain the delay in number of cycles at 20 kHz for early slip band formation. This delay can be quantitatively predicted. The dominant mechanism responsible for the frequency effect is cross slip. Because the cycle involved for 20 kHz fatigue tests is 200 times shorter than for 100 Hz loading, the cumulated cross-slip probability per cycle is 200 times lower. As a result, 200 times more cycles are needed for slip band emergence. This is consistent with the fact that strain localization and slip irreversibility due to cross slip are the early mechanisms needed to extrusion and so occur earlier and at lower stress amplitudes than production and diffusion of vacancies. Nevertheless, note that both mechanisms are coupled.

5. Conclusion

The impact of frequency on the fatigue response of copper polycrystal was investigated. It was shown that 100 Hz fatigue tests induce shorter fatigue life than 20 kHz tests. The final crack results from the emergence of slip bands at the specimen surface. The following conclusions can be made from the above obtained results:

- From optical observations it was evidenced that the loading frequency impacts the kinetics of slip band emergency.
- This frequency effect was attributed to two key time-dependent mechanisms in persistent slip band formation and extrusion growth: cross slip of screw dislocations and production/diffusion of vacancies.
- By varying the loading frequency the cycle period is 200 times longer at 100 Hz than 20 kHz which increase the probability of occurrence of each phenomenon: frequency increase reduces the cross-slip probability and the time for point defect diffusion over one cycle.
- By means of two simplified literature models, the delay in number of cycles was predicted and quantified for the first time and found in very good agreement with experimental results. Cross slip was found to be the dominant mechanism for slip band emergence.

These results, supported by both experimental and analytical analyses, explain the reasons for frequency effects observed on a material where slip band formation dominates the crack initiation process. It is believed that the obtained results could be extended to a large class of materials with similar fatigue crack initiation mechanisms (crack initiation from slip bands, type I materials). These results also suggest that in the case of materials with less pronounced plastic activity at crack initiation in the VHCF regime (High Strength Steels for example considered as type II materials), less or no frequency effect should be observed. In addition, the reasons for a possible frequency effect in the case of type II materials may be different. The later statements seem to correlate the existing literature on the subject, however further work is needed to fully address this aspect.

Data availability statement

The raw/processed data required to reproduce these findings cannot be shared at this time as the data also forms part of an ongoing study.

Acknowledgements

We would like to acknowledge the Agence Nationale de la Recherche France ANR-09-BLAN-0025-01 and the Ecole Doctorale SMI ENSAM for the funding that enabled this work to be carried, Griset company for supplying copper, Guillaume Thoquenne from CETIM which provides the failure S–N at 20 Hz and Nicolas Ranc for its help in fatigue measurements.

References

[1] C. Bathias, P. Paris, Gigacycle Fatigue in Mechanical Practice, M. CRC Press, Dekker, 2004.

[2] H. Mayer, M. Papakyriacou, R. Pippan, S. Stanzl-Tschegg, «Influence of loading frequency on the high fatigue properties of AlZnMgCu1.5 aluminium alloy», Mater Eng. Sci.A. 314 (2001) 48–54, https://doi.org/10.1016/S0921-5093(00)01913-4.

[3] M. Papakyriacou, H. Mayer, C. Pypen, J.H. Plenk, S. Stanzl-Tschegg, «Influence of loading frequency on high cycle fatigue properties of b.c.c and h.c.p metals», Mater. Sci. Eng. A 308 (2001) 143–152, https://doi.org/10.1016/s0921-5093(00)01978-x.

[4] R.J. Morrissey, D.L. McDowell, T. Nicholas, «Frequency and stress ratio effects in high cycle fatigue og Ti-6Al-4V», Int. J. Fatigue 21 (1999) 679–685, https://doi.org/10.1016/s0142-1123(99)00030-4.

[5] N. Tsutsumi, Y. Murakami, V. Doquet, «Effect of test frequency on fatigue strength of low carbon steel», Fatigue Fract. Eng. Mater. Struct. 32 (2009) 473–783, https://doi.org/10.1111/j.1460-2695.2009.01350.x.

[6] N. Torabian, V. Favier, J. Dirrenberger, F. Adamski, S. Ziaei-Rad, N. Ranc, «Correlation of the High and Very High Cycle Fatigue Response of Ferrite Based Steels with Strain Rate-Temperature Conditions» *Acta Materialia*, 2017, pp. 40–52, https://doi.org/10.1016/j.actamat.2017.05.064.

[7] A.W. Thompson, W.A. Backofen, «The effect of grain size on fatigue», Acta Metall. 19 (1971) 597–606, https://doi.org/10.1016/0001-6160(71)90012-5.

[8] J. Polák, M. Klesnil, P. Lukáš, «High cycle plastic stress-strain response of metals», Mater. Sci. Eng. 15 (1974) 231–237, https://doi.org/10.1016/0025-5416(74)90056-1.

[9] P. Lukáš, M. Klesnil, J. Polák, «High cycle fatigue life of metals», Mater. Sci. Eng. 15 (1974) 239–245, https://doi.org/10.1016/0025-5416(74)90057-3.

[10] P. Lukáš, L. Kunz, «Effect of grain size on the high cycle fatigue behaviour of polycristalline copper», Mater. Sci. Eng. 85 (1987) 67–75, https://doi.org/10.1016/0025-5416(87)90468-X.

[11] S. Stanzl-Tschegg, «Influence of material properties and testing frequency on VHCF and HCF lives of polycrystalline copper», Int. J. Fatigue 105 (2017) 86–96, https://doi.org/10.1016/j.ijfatigue.2017.08.014.

[12] N. Thompson, N. Wadsworth, N. Louat, «The origin of fatigue fracture in copper,», Philos. Mag. 1 (1956) 113–126, https://doi.org/10.1080/14786435608238086.

[13] S. Stanzl-Tschegg, H. Mughrabi, B. Schönbauer, «Life-time and cyclic slip of copper in the VHCF-regime», Int. J. Fatigue 29 (2007) 2050–2059, https://doi.org/10.1016/j.ijfatigue.2007.03.010.

[14] S.E. Stanzl-Tschegg, B. Schönbauer, «Mechanisms of strain localization, crack initiation and fracture of polycrystalline copper in the VHCF regime», Int. J. Fatigue 32 (2010) 886–893, https://doi.org/10.1016/j.ijfatigue.2009.03.016.

[15] N.L. Phung, V. Favier, N. Ranc, F. Vales, H. Mughrabi, «Very high cycle fatigue of copper: evolution, morphology and locations of surface slip markings», Int. J. Fatigue 63 (2014) 68–77, https://doi.org/10.1016/j.ijfatigue.2014.01.007.

[16] J. Awatani, K. Katagiri, A. Omura, T. Shiraishi, «A study of the fatigue limit of copper», Metall. Trans. 6A (1975) 1029–1034, https://doi.org/10.1007/bf02645527.

[17] P. Lukáš, L. Kunz, L. Navrátilová, O. Boku vka, «Fatigue damage of ultrafine-grain copper in very-high cycle fatigue region», Mater. Sci. Eng. A 528 (2011) 7036–7040, https://doi.org/10.1016/j.msea.2011.06.001.

[18] N.L. Phung, «Fatigue sous très faibles amplitudes de contrainte : analyse des mécanismes précurseurs de l'amorçage de fissures dans le cuivre polycristallin,» PhD Thesis, Arts et Metiers ParisTech, Paris, 2012.

[19] N. Ranc, V. Favier, B. Munier, F. Vales, G. Thoquenne, F. Lefebvre, «Thermal Response of C45 Steel in High and Very High Cycle Fatigue», Procedia.Eng vol. 133 (2015) 265–271, https://doi.org/10.1016/j.proeng.2015.12.668.

[20] H. Mughrabi, «On 'multi-stage' fatigue life diagram and the relevant life-controlling mechanisms in ultrahigh-cycle fatigue», Fatigue Fract. Eng. Mater. Struct. vol. 25 (2002) 755–764, https://doi.org/10.1046/j.1460-2695.2002.00550.x.

[21] J. Man, K. Obrtlik, J. Polak, «Extrusions and intrusions in fatigued metals. Part 1. State of the art and history», Philosopical.Mag. 86 (2009) 1295–1336, https://doi.org/10.1080/14786430902917616.

[22] W. Jia, J. Fernandes, «Mechanical behaviour and the evolution of the dislocation structure of copper polycrystal deformed under fatigue–tension and tension-fatigue sequential strain paths», Mater.Eng. Sci.A. 348 (2003) 133–144, https://doi.org/10.1016/s0921-5093(02)00630-5.

[23] K. Agbessi, «Approches expérimentales et multi-échelles des processus d'amorçage des fissures de fatigue sous chargements complexes,», PhD thesis, Arts et Metiers ParisTech, France, 2013.

[24] Q. Wei, «Strain rate effects in the ultrafine grain and nanocrystalline regimes—influence on some constitutive responses», J. Mater. Sci. 42 (2007) 1709–1727, https://doi.org/10.1007/s10853-006-0700-9.

[25] R.P. Carreker Jr., W.R. Hibbard Jr., «Tensile deformation of high-purity copper as a function of temperature, strain rate, and grain size», Acta Metall. 1 (1953) 657–663, https://doi.org/10.1016/0001-6160(53)90022-4.

[26] S. Suresh, Fatigue of Materials, 1998. Cambridge.

[27] P. Neumann, A. Tonnessen, Crack Initiation at Grain Boundaries in FCC Materials –Strength of Metals and Alloys, vol. 1, Pergamon Press, Oxfoxd, 1988, pp. 743–748.

[28] L. Llanes, C. Laird, «The role of annealing twin boundaries in the cyclic deformation of f.c.c. materials», Mater. Sci. Eng. A 157 (1992) 21–27, https://doi.org/10.1016/0921-5093(92)90094-h.

[29] J. Polák, A. Vasek, «Fatigue damage in polycrystalline copper below the fatigue limit», Int. J. Fatigue 16 (1994) 403–408, https://doi.org/10.1016/0142-1123(94)90453-7.

[30] P. Peralta, C. Laird, T. Mitchell, «Fatigue Fracture at Copper Bicrystal Interfaces: Fractography», Mater. Sci. Eng. A vol. 264 (1999) 215–231, https://doi.org/10.1016/s0921-5093(98)01088-0.

[31] N.L. Phung, V. Favier, N. Ranc, «Evaluating Schmid criterion for predicting preferential locations of persistent slip markings obtained after very high cycle fatigue for polycrystalline pure copper», Int. J. Fatigue 77 (2015) 115–127, https://doi.org/10.1016/j.ijfatigue.2015.03.009.

[32] V. Favier, A. Blanche, C. Wang, N.L. Phung, N. Ranc, D. Wagner, C. Bathias, A. Chrysochoos, H. Mughrabi, «Very high cycle fatigue for single phase ductile materials: comparison between α-iron, copper and α-brass polycrystals», Int. J. Fatigue 93 (2016) 326–338, https://doi.org/10.1016/j.ijfatigue.2016.05.034.

[33] L.D. Roth, L.E. Willertz, T.R. Leax, «On the Fatigue of Copper up to Ultrasonic Frequencies» in First International Conference On Fatigue And Corrosion Fatique Up to Ultrasonic Frequencies, Champion, PA, 1981.

[34] S.J. Basinski, Z.S. Basinski, A. Howie, «Early stages of fatigue in copper single crystals», Philos. Mag. 19 (1969) https://doi.org/10.1080/14786436908225856, 899-824.

[35] B. Devincre, L.P. Kubin, «Mesoscopic simulations of dislocations and plasticity», Mater Eng. Sci.A. 2234-236 (1997) 8–14, https://doi.org/10.1016/s0921-5093(97)00146-9.

[36] C. Déprès, C.F. Robertson, M.C. Fivel, «Low-strain fatigue in AISI 316L steel surface grains: a three-dimensional discrete dislocation dynamics modelling of the early cycles I. Dislocation microstructures and mechanical behaviour», Philos. Mag 84 (2004) 2257–2275, https://doi.org/10.1080/14786430410001690051.

[37] U. Essmann, U. Gösele, H. Mughrabi, «A model of extrusions and intrusions in fatigued metals I. Point-defect production and the growth of extrusions», Philos. Mag.A 44 (1981) 405–426, https://doi.org/10.1080/01418618108239541.

[38] J. Polák, «On the role of point defects in fatigue crack initiation», Mater. Sci. Eng. 92 (1987) 71–80, https://doi.org/10.1016/0025-5416(87)90157-1.

[39] J. Polák, M. Sauzay, «Growth of Extrusions in Localized Cyclic Plastic Straining», Mater. Eng. Sci.A. 500 (2009) 122–129, https://doi.org/10.1016/j.msea.2008.09.022.

[40] M. Verdier, M. Fivel, I. Groma, «Mesoscopic scale simulation of dislocation dynamics in fcc metals: principles and applications», Model.Simulat.Mater. Sci. Eng. 6 (1998) 755, https://doi.org/10.1088/0965-0393/6/6/007.

[41] J. Polák, J. Man, «Fatigue crack initiation – the role of point defects», Int. J. Fatigue 65 (2014) 18–27, https://doi.org/10.1016/j.ijfatigue.2013.10.016.

[42] J. Askill, Tracer Diffusion Data for Metals, Alloys and Simple Oxides, IFI/Plenum, New York, 1970.